

Optimized Spline Interpolation

Ramtin Madani, *Student Member, IEEE*, Ali Ayremlou, *Student Member, IEEE*, Arash Amini, Farrokh Marvasti, *Senior Member, IEEE*,

Abstract—In this paper, we investigate the problem of designing compact support interpolation kernels for a given class of signals. By using calculus of variations, we simplify the optimization problem from an infinite nonlinear problem to a finite dimensional linear case, and then find the optimum compact support function that best approximates a given filter in the least square sense (ℓ_2 norm). The benefit of compact support interpolants is the low computational complexity in the interpolation process while the optimum compact support interpolant guarantees the highest achievable Signal to Noise Ratio (SNR). Our simulation results confirm the superior performance of the proposed splines compared to other conventional compact support interpolants such as cubic spline.

Index Terms—Spline, Interpolation, Filter Design

I. INTRODUCTION

DUE the existence of powerful digital tools, nowadays it is very common to convert the continuous time signals into the discrete form, and after processing the discrete signal, we can convert the discrete signal back to the original domain. The conversion of the continuous signal into the discrete domain is usually called the sampling process; the common form of sampling consists of taking samples directly from the continuous signal at equidistant time instants (uniform sampling). Although the samples are uniquely determined by the continuous function, there are infinite number of continuous signals which produce the same set of samples. The reconstruction process is defined as selecting one of the infinite possibilities which satisfies certain constraints. For a given set of constraints, a proper sampling scheme is the one that establishes a one-to-one mapping between the discrete signals and the set of continuous functions that satisfy the constraints. One of the well-known constraints is the (finite support in fourier domain) condition [?]. Due to the advances in the wavelet theory [?], [?], [?], a new interest in continuous-time modeling and spline interpolation has been generated. Multiresolution analysis [?], [?], self-similarity [?], [?], and singularity analysis [?] are inseparable from a continuous-time interpolation. Although proper sampling schemes provide a one-to-one mapping between the continuous and discrete forms, we still need the tools to recover a continuous time signal from its samples. In fact, interpolation techniques using splines are one of the best options here.

In this field, polynomial splines, such as B-Splines, are particularly popular; mainly due to their simplicity, compact support, and excellent approximation capabilities compared to

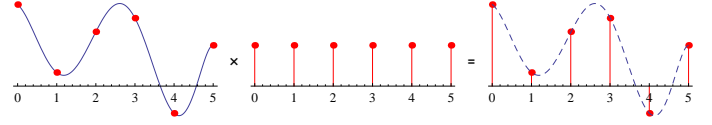


Fig. 1. Sampling process modeled by multiplying an impulse train by a continuous time signal.

other methods. B-Spline interpolations have spread to various applications [?], [?], [?].

Many advantages of the B-splines arise from the fact that they are compact support functions. However, there is no evidence that they are the best compact support kernels for the interpolation process; i.e., it may be possible to improve the performance without compromising the desired property of the compact supportedness. In this paper, we focus on the problem of designing compact support splines that best resemble a given filter such as the ideal lowpass filter; more precisely, we aim to find a compact support spline that minimizes the least squared error when its cardinal spline is compared to a given function. The given filter may be any arbitrary function that reflects the properties and constraints of the class of signals that enter the sampling process.

The remainder of the paper is organized as follows: The next section briefly describes the spline interpolation method. In section III, a novel scheme is proposed to produce new optimized splines for interpolation regardless of the type of filtering. The performance of the proposed method is evaluated in section IV by comparing the interpolation results of the proposed method to those of well-known interpolation techniques. Section V concludes the paper.

II. PRELIMINARIES

In this paper, the following notations and definitions are used:

Definition 1. For a continuous-time signal $x(t)$, a continuous-time signal $x_p(t)$ and a discrete-time signal $x_d[n]$ are defined as follows:

$$x_d[n] \triangleq x(nT) \quad (1)$$

$$x_p(t) \triangleq x(t)p(t) = \sum_{n=-\infty}^{\infty} x_d[n]\delta(t - nT) \quad (2)$$

where $p(t) \triangleq \sum_{n=-\infty}^{+\infty} \delta(t - nT)$ is the periodic impulse train. The sampling period T is normalized to 1 without any loss of generality.

The sampling process is shown in Fig 1.

All authors are with Advanced Communications Research Institute (ACRI), the Department of Electrical Engineering, Sharif University of Technology, Tehran, Iran, e-mails: {r_madani, a_ayremlou, arashsil}@ee.sharif.edu, marvasti@sharif.ir

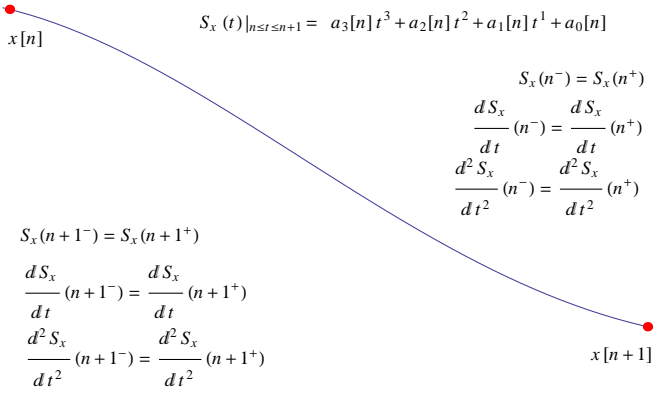


Fig. 2. Spline of the degree 3 conditions.

Definition 2. A Linear Time Invariant (LTI) filter with impulse response $h(t)$ is called to have interpolation property if and only if,

$$h_p(t) = \delta(t). \quad (3)$$

Definition 3. For a continuous-time signal $x(t)$ and any odd integer m , $x_s^m(t)$ is a polynomial spline of degree m if,

- 1) for any $n \in \mathbb{Z}$, $x_s^m(t)$ is a polynomial of (at most) degree m in the interval $[n, n+1]$ (Compact support),
- 2) for any $n \in \mathbb{Z}$, $x_s^m(n) = x_d[n]$ (Interpolation property),
- 3) $x_s^m \in C^{m-1}(-\infty, \infty)$ (Smoothness).

According to the first property, $(m+1)^{th}$ derivative of x_s^m is equal to an impulse train.

Definition 4. For the polynomial spline $x_s^m(t)$, the polynomial spline coefficients $\dot{x}_d^m[n]$ are defined as:

$$\dot{x}_p^m(t) = \sum_{n=-\infty}^{\infty} \dot{x}_d^m[n] \delta(t-n) \triangleq \frac{d^{m+1}}{dt^{m+1}} x_s^m(t) \quad (4)$$

To determine all polynomials of degree m that form $x_s^m(t)$, the $m+1$ unknown spline coefficients should be found in order to satisfy the conditions 2 and 3 (Fig. 2). If the goal is to discover a piecewise polynomial signal that is $(m-1)$ times differentiable with continuous derivatives, a natural method is to derive $\dot{x}_d^m[n]$ according to $x_d[n]$ and then calculate the integral of $\dot{x}_x^m(t)$, $m+1$ times, i.e.,

$$\begin{aligned} x_s^m(t) &= \int_{-\infty}^t \int_{-\infty}^{t_m} \dots \int_{-\infty}^{t_1} \dot{x}_p^m(t_0) dt_0 \dots dt_{m-1} dt_m \\ &= (u^{m+1} * \dot{x}_p^m)(t) \end{aligned} \quad (5)$$

where $u^1(t)$ is the unity step function and for any $k \in \mathbb{N}$, $u^{k+1}(t) \triangleq (u^k * u^1)(t)$.

Lemma 1. If the Region Of Convergence (ROC) of $X_d^m(z)$ is not enclosed in the unit circle (i.e., there exists $z \in ROC\{X_d^m\}$ such that $|z| > 1$), then from Def. 3, $x_s^m(t)$ will be uniquely determined from $x_d[n]$, and

$$x_s^m(t) = ((u^{m+1} * (u_p^{m+1})^{-1}) * x_p)(t) \quad (6)$$

where $(u_p^{m+1})^{-1}(t)$ is defined as the inverse of $u_p^{m+1}(t)$, i.e., $((u_p^{m+1})^{-1} * u_p^{m+1})(t) = \delta(t)$, and $X_d^m(z)$ is the z-transform of $x_d^m[n]$.

Proof: From Def. 4,

$$\begin{aligned} x_p^m(t) &= x_s^m(t)p(t) \\ &= (u^{m+1} * \dot{x}_p^m)(t)p(t) \\ &= (u_p^{m+1} * \dot{x}_p^m)(t) \end{aligned} \quad (7)$$

Hence,

$$x_d^m[n] = (u_d^{m+1} * \dot{x}_d^m)[n] \quad (8)$$

The ROC of $U_d^{m+1}(z)$ is $|z| > 1$ and there are no zeros in this region. Since the ROC of $X_d^m(z)$ is not enclosed in the unit circle, $(U_d^{m+1})^{-1}(z)$ and $X_d^m(z)$ have a region in common. Thus,

$$\dot{x}_p^m(t) = ((u_p^{m+1})^{-1} * x_p^m)(t) \quad (9)$$

and according to (5),

$$\begin{aligned} x_s^m(t) &= (u^{m+1} * \dot{x}_p^m)(t) \\ &= (u^{m+1} * (u_p^{m+1})^{-1} * x_p^m)(t) \end{aligned} \quad (10)$$

Definition 5. A discrete-time signal $y_d[n]$ is called a proper signal if and only if it is bounded and has a unique and bounded inverse $y_d^{-1}[n]$.

Definition 6. For any continuous-time signal $y(t)$, if $y_d[n]$ is a proper signal, then $\hat{y}(t)$ is defined as follows:

$$\hat{y}(t) = ((y_p)^{-1} * y)(t) \quad (11)$$

Corollary 1. $\hat{y}(t)$ in (11) is the impulse response of a filter with interpolation property, in other words:

$$\hat{y}_p(t) = \delta(t) \quad (12)$$

Proof:

$$\begin{aligned} \hat{y}_p(t) &= \hat{y}(t)p(t) \\ &= [((y_p)^{-1} * y)(t)]p(t) \\ &= ((y_p)^{-1} * y_p)(t) = \delta(t) \end{aligned} \quad (13)$$

Lemma 2. For a given proper signal $y_d^m[n]$, the signal $\hat{y}_s^m(t)$ is only a function of m and does not depend on $y_d^m[n]$.

Proof:

$$\begin{aligned} \hat{y}_s^m(t) &= ((y_s^m)_p)^{-1} * y_s^m(t) \\ &= ((y_p)^{-1} * y_s^m)(t) \\ &= ((y_p)^{-1} * (u^{m+1} * (u_p^{m+1})^{-1}) * y_p)(t) \\ &= (u^{m+1} * (u_p^{m+1})^{-1})(t) \end{aligned} \quad (14)$$

Hence $\hat{y}_s^m(t)$ is only a function of m .

Definition 7. According to the above corollary, $c^m(t) \triangleq \widehat{y_s^m}(t)$ is defined as the cardinal spline of degree m (Fig. 3).

From (6) and (14) it can be concluded that the polynomial spline interpolation is a linear shift invariant process according to $x_d[n]$ and its impulse response is represented by $c^m(t)$. $c^m(t)$, on the other hand, can be derived according to any arbitrary polynomial spline $y_s^m(t)$ such that $y_d^m(t)$ is a proper signal, i.e.,

$$\begin{aligned} x_s^m(t) &= (c^m * x_p)(t) \\ &= (y_s^m * ((y_p)^{-1} * x_p))(t) \end{aligned} \quad (15)$$

The above equation divides the whole interpolation process into a discrete-time and a continuous-time section. If $y_s^m(t)$ is chosen as a time limited basis, both sections of this process can be extremely simplified and a considerable amount of continuous-time calculation can be avoided.

Theorem 1. $k = m + 1$ is the least positive integer for which there exists a polynomial spline of degree m , such as $y_s^m(t)$, that vanishes outside the interval $(0, k)$, i.e.,

$$\forall t \notin (0, k) \Rightarrow y_s^m(t) = 0 \quad (16)$$

then $k = m + 1$.

Proof: Suppose that $y_s^m(t)$ satisfies (16) and $\dot{Y}_d^m(z)$ is the z-transform of $\dot{y}_d^m[n]$, where $\dot{y}_d^m[n]$ is the coefficients signal for the polynomial spline $y_s^m(t)$ according to the definition (4). It can be claimed that,

$$(z - 1)^{m+1} \mid \dot{Y}_d^m(z^{-1}) \quad (17)$$

In order to prove (17), we define the sequence of polynomials $\{Q_i\}_{i=0}^m$ such that $Q_0(z) \triangleq \dot{Y}_d^m(z^{-1})$ and for $1 \leq n \leq m$,

$$Q_i \triangleq z \frac{d}{dz} Q_{i-1} = \sum_{n=0}^k \dot{y}_d^m[n] n^i z^n \quad (18)$$

Also polynomial H is defined as follows:

$$\begin{aligned} H(t) &\triangleq \frac{1}{m!} \sum_{i=0}^m (-1)^i Q_i(1) \binom{m}{i} t^{m-i} \\ &= \frac{1}{m!} \sum_{i=0}^m (-1)^i \left(\sum_{n=0}^k \dot{y}_d^m[n] n^i \right) \binom{m}{i} t^{m-i} \\ &= \frac{1}{m!} \sum_{n=0}^k \dot{y}_d^m[n] \sum_{i=0}^m \binom{m}{i} (-1)^i n^i t^{m-i} \\ &= \frac{1}{m!} \sum_{n=0}^k \dot{y}_d^m[n] (t - n)^m \end{aligned} \quad (19)$$

Thus, according to (5), for any $t > k$, $H(t)$ is equal to $y_s^m(t)$, i.e.,

$$\forall t > k \Rightarrow H(t) = y_s^m(t) = 0 \quad (20)$$

Since H is a polynomial that vanishes for infinite values of t , it should be equivalent to zero:

$$H(t) \equiv 0 \Rightarrow Q_m(1) = Q_{m-1}(1) = \dots = Q_0(1) = 0 \quad (21)$$

From the above equations, it is concluded directly by induction that,

$$\forall n \in \mathbb{N}; 0 \leq n \leq m \Rightarrow \frac{d^n}{dz^n} \dot{Y}_d^m(z^{-1}) \Big|_{z=1} = 0 \quad (22)$$

Hence, $(z - 1)^{m+1}$ divides $\dot{Y}_d^m(z^{-1})$. On the other hand, since $\dot{Y}_d^m(z^{-1}) = \sum_{n=0}^k \dot{y}_d^m[n] z^n$, (17) shows that $\dot{y}_d^m[m+1] \neq 0$. Hence,

$$y_s^m(t) \Big|_{t \in (m+1-\epsilon, m+1+\epsilon)} \neq 0 \quad (23)$$

Thus $k \geq m + 1$.

Finally, it must be shown that there exists a polynomial spline of degree m that is supported in the interval $(0, m + 1)$. Suppose that $\dot{Y}_d^m(z) = (z^{-1} - 1)^{m+1}$, then

$$\Rightarrow y_d^m[n] = (-1)^n \binom{m+1}{n} \quad (24)$$

$$\Rightarrow y_s^m(t) = u^{m+1} * \left[\sum_{n=0}^{m+1} y_d^m[n] \delta(t - n) \right] \quad (25)$$

$$\Rightarrow y_s^m(t) = \sum_{n=0}^{m+1} y_d^m[n] u^{m+1}(t - n). \quad (26)$$

Thus, for all $t \geq m + 1$, $y_s^m(t) = 0$. ■

Definition 8. The polynomial B-Spline of degree m is defined as follows:

$$\beta^m(t) \triangleq \sum_{n=0}^{m+1} (-1)^n \binom{m+1}{n} u^{m+1}(t - n) \quad (27)$$

Now according to the lemma 2, the polynomial spline interpolation process can be implemented by a compact support kernel such as the polynomial B-Splines, i.e.,

$$\dot{x}_d^m[n] = \left((\beta_d^m)^{-1} * x_d^m \right)[n] \quad (28)$$

$$x_s^m(t) = \sum_{n=-\infty}^{\infty} \dot{x}_d^m[n] \beta^m(t - n) \quad (29)$$

III. PROPOSED OPTIMIZED B-SPLINE

In many applications, it is desirable that the interpolation filter resembles an ideal filter, and the second and third properties in Def. 3 may be ignored. In this section an optimized basis spline will be introduced to emulate a desired filter.

Definition 9. Let D denote the set of all continuous-time signals that satisfy the dirichlet conditions, i.e., for any $y(t) \in D$

- 1) $y(t)$ has a finite number of extrema in any given interval,
- 2) $y(t)$ has a finite number of discontinuities in any given interval,
- 3) $y(t)$ is absolutely integrable over a period,
- 4) $y(t)$ is bounded.

First of all, an affine subspace of all signals that satisfy the dirichlet conditions will be defined, and then the optimized solution will be obtained in this set by the calculus of variation.

Definition 10. Let $y_d[n]$ be a proper signal that vanishes for all $n \leq 0$ and $n \geq m + 1$, then $\chi^m(y_d)$ is the set of all continuous-time signals $y(t)$ that satisfy the following conditions,

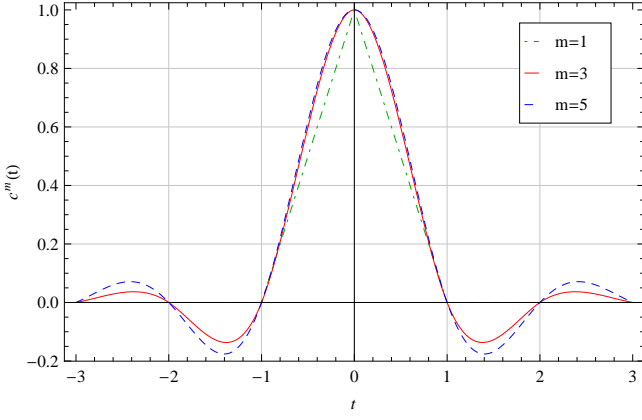


Fig. 3. Cardinal splines of different degrees.

- 1) $y \in D$
- 2) $\forall n \in \mathbb{N}; y(n) = y_d[n]$
- 3) $\forall t \notin (0, m+1); y(t) = 0$

The use of $y(t) \in \chi^m(y_d)$ as a basis spline to interpolate $x_d[n]$ according to equations (28) and (29) is a linear time invariant process with the impulse response $\hat{y}(t)$.

Definition 11. The error function $e_x: \chi^m(y_d) \rightarrow \mathbb{R}$ is defined as follows:

$$\begin{aligned}
 e_x(y) &\triangleq \|\hat{y} * x_p - x\|_2 \\
 &= \int_{-\infty}^{\infty} |(\hat{y} * x_p)(t) - x(t)|^2 dt \\
 &= \int_{-\infty}^{\infty} |\mathcal{F}\{\hat{y} * x_p\} - \mathcal{F}\{x\}|^2 df \\
 &= \int_{-\infty}^{\infty} |\mathcal{F}\{((y_p)^{-1} * y) * x_p\} - \mathcal{F}\{x\}|^2 df \\
 &= \int_{-\infty}^{\infty} \left| \frac{\mathcal{F}\{x_p\}}{\mathcal{F}\{y_p\}} \mathcal{F}\{y\} - \mathcal{F}\{x\} \right|^2 df. \quad (30)
 \end{aligned}$$

where \mathcal{F} is defined as the continuous time Fourier transform operator.

Definition 12. According to the above definition, if ρ_d^m is a proper signal that vanishes for all $n \leq 0$ and $n \geq m+1$, an optimized basis spline $\rho^m[x, \rho_d^m]$ is defined as follows:

$$\rho^m[x, \rho_d^m] \triangleq \arg \min_{y \in \chi^m(\rho_d^m)} e_x(y) \quad (31)$$

Now, for a given proper discrete signal ρ_d^m with the required vanishing property, we employ the calculus of variations in order to find the optimized continuous basis spline ρ^m that minimizes the error function $e_x(\rho^m)$.

Theorem 2. Equation (31) has a unique solution that satisfies the following property,

$$[x_p * \overline{x_p} * (\rho_p^m)^{-1} * (\overline{\rho_p^m})^{-1}] * \rho^m = [(\overline{\rho_p^m})^{-1} * \overline{x_p}] * x \quad (32)$$

for all $t \in (0, m+1)$, where $\overline{y}(t) \triangleq y^*(-t)$.

Proof: For $\gamma \in \chi^m(0)$ and any $\varepsilon > 0$, we have $\rho^m + \varepsilon\gamma \in \chi^m(\rho_d^m)$, and the variational derivation of $e_x(\rho^m)$ with respect

to ρ^m with γ as the test function is equal to

$$\begin{aligned}
 \langle e_x(\rho^m), \gamma \rangle &\triangleq \lim_{\varepsilon \rightarrow 0} \frac{e_x(\rho^m + \varepsilon\gamma) - e_x(\rho^m)}{\varepsilon} \\
 &= 2 \int_{-\infty}^{\infty} \Re\{\gamma(t)\} \Re\left\{ \mathcal{F}^{-1} \left\{ \left[\frac{\mathcal{F}\{x_p\}}{\mathcal{F}\{\rho_p^m\}} \right]^* \right. \right. \\
 &\quad \left. \left. \left[\frac{\mathcal{F}\{\rho^m\}}{\mathcal{F}\{\rho_p^m\}} \mathcal{F}\{x_p\} - \mathcal{F}\{x\} \right] \right\} \right\} dt \\
 &\quad - 2 \int_{-\infty}^{\infty} \Im\{\gamma(t)\} \Im\left\{ \mathcal{F}^{-1} \left\{ \left[\frac{\mathcal{F}\{x_p\}}{\mathcal{F}\{\rho_p^m\}} \right]^* \right. \right. \\
 &\quad \left. \left. \left[\frac{\mathcal{F}\{\rho^m\}}{\mathcal{F}\{\rho_p^m\}} \mathcal{F}\{x_p\} - \mathcal{F}\{x\} \right] \right\} \right\} dt \quad (33)
 \end{aligned}$$

The proof of (33) is presented in (34). Since $\chi^m(\rho_d^m)$ is boundless, in order to minimize $e_x(\rho^m)$, $\langle e(\rho^m), \gamma \rangle$ should be zero for all $\gamma \in \chi^m(0)$, which implies that the second term inside the integrals should be zero for $t \in (0, m+1)$, i.e.,

$$\mathcal{F}^{-1} \left\{ \left[\frac{\mathcal{F}\{x_p\}}{\mathcal{F}\{\rho_p^m\}} \right]^* \left[\frac{\mathcal{F}\{\rho^m\}}{\mathcal{F}\{\rho_p^m\}} \mathcal{F}\{x_p\} - \mathcal{F}\{x\} \right] \right\} = 0 \quad (35)$$

The above equation directly yields (32). ■

Thus, it is proven that the optimized basis spline which gives the best estimation of x , should satisfy (32). By defining

$$v_p(t) \triangleq (x_p * \overline{x_p}) * [(\rho_p^m)^{-1} * (\overline{\rho_p^m})^{-1}] \quad (36)$$

$$w(t) \triangleq [(\overline{\rho_p^m})^{-1} * \overline{x_p}] * x, \quad (37)$$

we can rewrite (32) as $(v_p * \rho^m)(t) = w(t)|_{t \in (0, m+1)}$. Since this equation is only valid in a particular interval, $(v_p)^{-1}$ cannot be used to obtain ρ^m . However, since v_p is an impulse train (convolution of four impulse trains) we will show that the continuous functional equation in (32) boils down to solving a finite Hermitian system of linear equations. For this purpose, we first define the two following sequences of functions which are supported only on a unit-length interval:

$$R_n(t) = \begin{cases} \rho^m(t+n) & 0 \leq t < 1 \\ 0 & \text{o.w.} \end{cases} \quad (38)$$

$$W_n(t) = \begin{cases} w(t+n) & 0 \leq t < 1 \\ 0 & \text{o.w.} \end{cases} \quad (39)$$

Now, here is (32) in the matrix form:

$$\begin{bmatrix} v_d[0] & v_d[-1] & \dots & v_d[-m] \\ v_d[1] & v_d[0] & \dots & v_d[-m+1] \\ \vdots & \vdots & \ddots & \vdots \\ v_d[m] & v_d[m-1] & \dots & v_d[0] \end{bmatrix} \begin{bmatrix} R_0 \\ R_1 \\ \vdots \\ R_m \end{bmatrix} = \begin{bmatrix} W_0 \\ W_1 \\ \vdots \\ W_m \end{bmatrix} \quad (40)$$

Since $v_d[-n] = v_d^*[n]$, the above matrix $V \triangleq [v_d[i-j]]_{i=1, \dots, m+1; j=1, \dots, m+1}$ is Hermitian also. Now by solving (40), $\{R_n\}_{n=0}^m$ is derived and thus the optimized basis spline is given as

$$\rho^m(t) = \sum_{n=0}^m R_n(t-n) \quad (41)$$

$$\begin{aligned}
\langle e_x(\rho^m[x, \rho_d^m]), \gamma \rangle &\triangleq \lim_{\varepsilon \rightarrow 0} \frac{e_x(\rho^m + \varepsilon\gamma) - e_x(\rho^m)}{\varepsilon} \\
&= \lim_{\varepsilon \rightarrow 0} \frac{1}{\varepsilon} \left[\int_{-\infty}^{\infty} \left| \left(\frac{\mathcal{F}\{\rho^m + \varepsilon\gamma\}}{\mathcal{F}\{(\rho^m + \varepsilon\gamma)p\}} \right) \mathcal{F}\{x_p\} - \mathcal{F}\{x\} \right|^2 df - \int_{-\infty}^{\infty} \left| \left(\frac{\mathcal{F}\{\rho^m\}}{\mathcal{F}\{\rho_p^m\}} \right) \mathcal{F}\{x_p\} - \mathcal{F}\{x\} \right|^2 df \right] \\
&= \lim_{\varepsilon \rightarrow 0} \frac{1}{\varepsilon} \int_{-\infty}^{\infty} \left\{ \left[\Re \left\{ \left(\frac{\mathcal{F}\{\rho^m + \varepsilon\gamma\}}{\mathcal{F}\{(\rho^m + \varepsilon\gamma)p\}} \right) \mathcal{F}\{x_p\} - \mathcal{F}\{x\} \right\}^2 - \Re \left\{ \left(\frac{\mathcal{F}\{\rho^m\}}{\mathcal{F}\{\rho_p^m\}} \right) \mathcal{F}\{x_p\} - \mathcal{F}\{x\} \right\}^2 \right] \right. \\
&\quad \left. + \left[\Im \left\{ \left(\frac{\mathcal{F}\{\rho^m + \varepsilon\gamma\}}{\mathcal{F}\{(\rho^m + \varepsilon\gamma)p\}} \right) \mathcal{F}\{x_p\} - \mathcal{F}\{x\} \right\}^2 - \Im \left\{ \left(\frac{\mathcal{F}\{\rho^m\}}{\mathcal{F}\{\rho_p^m\}} \right) \mathcal{F}\{x_p\} - \mathcal{F}\{x\} \right\}^2 \right] \right\} df \\
&= \lim_{\varepsilon \rightarrow 0} \frac{1}{\varepsilon} \int_{-\infty}^{\infty} \left\{ \Re \left\{ \left(\frac{\mathcal{F}\{\rho^m + \varepsilon\gamma\}}{\mathcal{F}\{(\rho^m + \varepsilon\gamma)p\}} - \frac{\mathcal{F}\{\rho^m\}}{\mathcal{F}\{\rho_p^m\}} \right) \mathcal{F}\{x_p\} \right\} \Re \left\{ \left(\frac{\mathcal{F}\{\rho^m + \varepsilon\gamma\}}{\mathcal{F}\{(\rho^m + \varepsilon\gamma)p\}} + \frac{\mathcal{F}\{\rho^m\}}{\mathcal{F}\{\rho_p^m\}} \right) \mathcal{F}\{x_p\} - 2\mathcal{F}\{x\} \right\} \right. \\
&\quad \left. + \Im \left\{ \left(\frac{\mathcal{F}\{\rho^m + \varepsilon\gamma\}}{\mathcal{F}\{(\rho^m + \varepsilon\gamma)p\}} - \frac{\mathcal{F}\{\rho^m\}}{\mathcal{F}\{\rho_p^m\}} \right) \mathcal{F}\{x_p\} \right\} \Im \left\{ \left(\frac{\mathcal{F}\{\rho^m + \varepsilon\gamma\}}{\mathcal{F}\{(\rho^m + \varepsilon\gamma)p\}} + \frac{\mathcal{F}\{\rho^m\}}{\mathcal{F}\{\rho_p^m\}} \right) \mathcal{F}\{x_p\} - 2\mathcal{F}\{x\} \right\} \right\} df \\
&= \lim_{\varepsilon \rightarrow 0} \frac{1}{\varepsilon} \int_{-\infty}^{\infty} \left\{ \Re \left\{ \left(\frac{\mathcal{F}\{\rho^m + \varepsilon\gamma\} - \mathcal{F}\{\rho^m\}}{\mathcal{F}\{\rho_p^m\}} \right) \mathcal{F}\{x_p\} \right\} \Re \left\{ \left(\frac{\mathcal{F}\{\rho^m + \varepsilon\gamma\} + \mathcal{F}\{\rho^m\}}{\mathcal{F}\{\rho_p^m\}} \right) \mathcal{F}\{x_p\} - 2\mathcal{F}\{x\} \right\} \right. \\
&\quad \left. + \Im \left\{ \left(\frac{\mathcal{F}\{\rho^m + \varepsilon\gamma\} - \mathcal{F}\{\rho^m\}}{\mathcal{F}\{\rho_p^m\}} \right) \mathcal{F}\{x_p\} \right\} \Im \left\{ \left(\frac{\mathcal{F}\{\rho^m + \varepsilon\gamma\} + \mathcal{F}\{\rho^m\}}{\mathcal{F}\{\rho_p^m\}} \right) \mathcal{F}\{x_p\} - 2\mathcal{F}\{x\} \right\} \right\} df \\
&= \lim_{\varepsilon \rightarrow 0} \frac{1}{\varepsilon} \int_{-\infty}^{\infty} \left\{ \Re \left\{ \left(\frac{\mathcal{F}\{\varepsilon\gamma\}}{\mathcal{F}\{\rho_p^m\}} \right) \mathcal{F}\{x_p\} \right\} \Re \left\{ \left(\frac{\mathcal{F}\{2\rho^m + \varepsilon\gamma\}}{\mathcal{F}\{\rho_p^m\}} \right) \mathcal{F}\{x_p\} - 2\mathcal{F}\{x\} \right\} \right. \\
&\quad \left. + \Im \left\{ \left(\frac{\mathcal{F}\{\varepsilon\gamma\}}{\mathcal{F}\{\rho_p^m\}} \right) \mathcal{F}\{x_p\} \right\} \Im \left\{ \left(\frac{\mathcal{F}\{2\rho^m + \varepsilon\gamma\}}{\mathcal{F}\{\rho_p^m\}} \right) \mathcal{F}\{x_p\} - 2\mathcal{F}\{x\} \right\} \right\} df \\
&= \int_{-\infty}^{\infty} \Re \left\{ \frac{\mathcal{F}\{\gamma\}}{\mathcal{F}\{\rho_p^m\}} \mathcal{F}\{x_p\} \right\} \Re \left\{ 2 \frac{\mathcal{F}\{\rho^m\}}{\mathcal{F}\{\rho_p^m\}} \mathcal{F}\{x_p\} - 2\mathcal{F}\{x\} \right\} + \Im \left\{ \frac{\mathcal{F}\{\gamma\}}{\mathcal{F}\{\rho_p^m\}} \mathcal{F}\{x_p\} \right\} \Im \left\{ 2 \frac{\mathcal{F}\{\rho^m\}}{\mathcal{F}\{\rho_p^m\}} \mathcal{F}\{x_p\} - 2\mathcal{F}\{x\} \right\} df \\
&= 2\Re \left\{ \int_{-\infty}^{\infty} \left[\frac{\mathcal{F}\{\gamma\}}{\mathcal{F}\{\rho_p^m\}} \mathcal{F}\{x_p\} \right] \left[\frac{\mathcal{F}\{\rho^m\}}{\mathcal{F}\{\rho_p^m\}} \mathcal{F}\{x_p\} - \mathcal{F}\{x\} \right]^* df \right\} \\
&= 2\Re \left\{ \int_{-\infty}^{\infty} \mathcal{F}\{\gamma\} \left[\frac{\mathcal{F}\{x_p\}}{\mathcal{F}\{\rho_p^m\}} \right] \left[\frac{\mathcal{F}\{\rho^m\}}{\mathcal{F}\{\rho_p^m\}} \mathcal{F}\{x_p\} - \mathcal{F}\{x\} \right]^* df \right\} \\
&= 2\Re \left\{ \int_{-\infty}^{\infty} \gamma(t) \mathcal{F}^{-1} \left\{ \left[\frac{\mathcal{F}\{x_p\}}{\mathcal{F}\{\rho_p^m\}} \right]^* \left[\frac{\mathcal{F}\{x_p\}}{\mathcal{F}\{\rho_p^m\}} \mathcal{F}\{\rho^m\} - \mathcal{F}\{x\} \right] \right\} dt \right\} \\
&= 2 \int_{-\infty}^{\infty} \Re \{ \gamma(t) \} \Re \left\{ \mathcal{F}^{-1} \left\{ \left[\frac{\mathcal{F}\{x_p\}}{\mathcal{F}\{\rho_p^m\}} \right]^* \left[\frac{\mathcal{F}\{x_p\}}{\mathcal{F}\{\rho_p^m\}} \mathcal{F}\{\rho^m\} - \mathcal{F}\{x\} \right] \right\} \right\} dt \\
&\quad - 2 \int_{-\infty}^{\infty} \Im \{ \gamma(t) \} \Im \left\{ \mathcal{F}^{-1} \left\{ \left[\frac{\mathcal{F}\{x_p\}}{\mathcal{F}\{\rho_p^m\}} \right]^* \left[\frac{\mathcal{F}\{x_p\}}{\mathcal{F}\{\rho_p^m\}} \mathcal{F}\{\rho^m\} - \mathcal{F}\{x\} \right] \right\} \right\} dt
\end{aligned} \tag{34}$$

This optimized basis spline minimizes the mean squared error of interpolation. On the other hand, smoothness of the optimized basis spline and causality of the prefilter can be achieved by adjusting ρ_d .

Another application of (32) is to approximate an ideal interpolation filter by an optimized basis spline. In fact, basis splines are superior to FIR filters.

Now the goal is to design ρ^m such that $\widehat{\rho^m}$ would be the best estimation of h , which denotes the impulse response of a filter that has the interpolation property.

Lemma 3. (Estimating a desired filter) Assume $h(t)$ is the impulse response of a linear time invariant filter which satisfies the interpolation property and let $\rho_d^m[n]$ be a proper discrete

signal, then,

$$\arg \min_{y \in \chi^m(\rho_d^m)} \|h - \widehat{y}\|_2 = \rho^m[h, \rho_d^m] \tag{42}$$

Proof:

$$\begin{aligned}
e_h(y) &= \int_{-\infty}^{\infty} |\mathcal{F}\{\widehat{y} * h_p\} - \mathcal{F}\{h\}|^2 df \\
&= \int_{-\infty}^{\infty} |\mathcal{F}\{\widehat{y}\} \mathcal{F}\{h_p\} - \mathcal{F}\{h\}|^2 df \\
&= \int_{-\infty}^{\infty} |\mathcal{F}\{\widehat{y}\} - \mathcal{F}\{h\}|^2 df \\
&= \|h - \widehat{y}\|_2^2
\end{aligned} \tag{43}$$

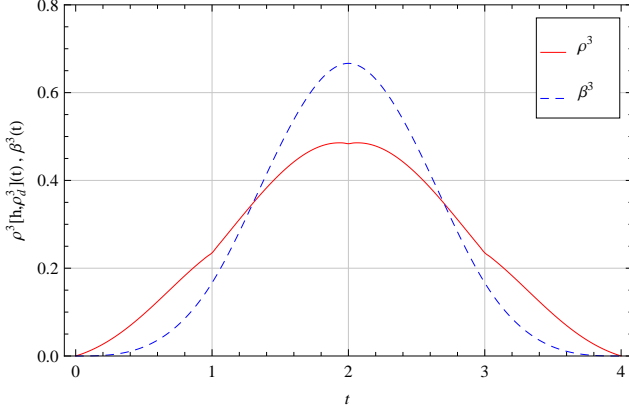


Fig. 4. The optimized spline versus cubic B-spline. $\rho^3\{h, \rho_d^3\}$ is the optimized basis spline built for estimating the ideal lowpass filter $h(t) = \frac{\sin(\pi t)}{\pi t}$ with $\rho_d^3(z) = 0.235z + 0.484z^2 + 0.235z^3$.

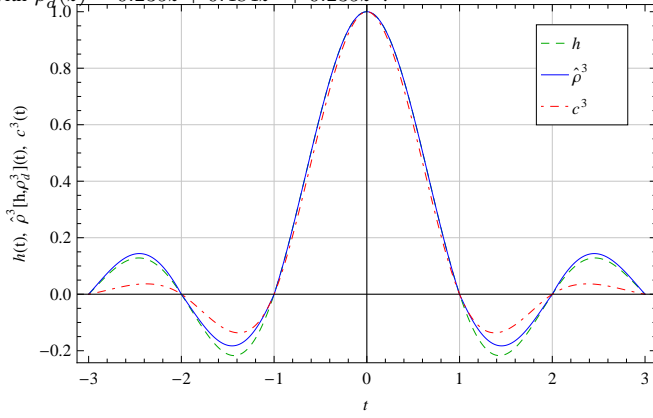


Fig. 5. The comparison of the proposed method with the cubic spline for an ideal lowpass filter.

Thus

$$\arg \min_{y \in \chi^m(\rho_d^m)} \|h - \hat{y}\|_2 = \arg \min_{y \in \chi^m(\rho_d^m)} e_h(y) = \rho^m[h, \rho_d^m] \quad (44)$$

Corollary 2. For an impulse response $h(t)$ with the interpolation property, if $\rho^m \in \chi^m(\rho_d^m)$ denotes the optimum basis spline for which $\hat{\rho}^m$ best approximates $h(t)$ (i.e., $\hat{\rho}^m(t) = \arg \min_{y \in \chi^m(\rho_d^m)} \|h - \hat{y}\|_2$), then $\rho^m \in \chi^m(\rho_d^m)$ satisfies:

$$[(\rho_p^m)^{-1} * (\overline{\rho_p^m})^{-1}] * \rho^m = [(\overline{\rho_p^m})^{-1}] * h \quad (45)$$

The proof follows directly from (32) and the fact that $h(t)$ has the interpolation property.

Figure 4 shows the cubic B-spline and the optimized B-spline designed for estimating the ideal lowpass filter $h(t) = \text{sinc}(t)$ with $\rho_d^3(z) = 0.235z + 0.484z^2 + 0.235z^3$, while Fig. 5 shows $\hat{\rho}^3[h, \rho_d^3](t)$ in comparison to $c^3(t)$.

IV. SIMULATION RESULTS

To compare the proposed method with the existing interpolation techniques, we have performed various simulations. The cubic B-spline, due to its short time support and relatively

high accuracy in approximating the ideal lowpass filter, is the most common technique for interpolating 1-D lowpass signals. For the purpose of comparison, we have optimized a spline function with the same time support as an ideal lowpass filter. Figures 4 and 5 show the shape of the obtained B-spline and the interpolating spline, respectively. Figure 4 shows that the energy is more concentrated in the middle of the cubic B-spline while the optimized spline has slower decaying rate of energy at the sides. The resultant interpolation splines, as depicted in Fig. 5, reveal that the main advantage of the optimized spline ($\hat{\rho}^3$) compared to the cubic spline (c^3), is the smaller error in the first side-lobe. The SNR values of $\hat{\rho}^3$ and c^3 with respect to the *sinc* function are 20.39 and 13.15dBs, respectively.

For a more realistic comparison, we have applied different interpolation techniques on standard test images. For this purpose, the original images, with or without applying the anti-aliasing filter (ideal lowpass filter), are down-sampled by a factor 2 in each direction (25% of the original pixels) and then they are enlarged (zooming) using the interpolation techniques. The comparison is made with the following interpolation methods: 1) bilinear interpolation, 2) bicubic interpolation, 3) wavelet-domain zero padding cycle-spinning [?], and 4) soft-decision estimation technique for adaptive image interpolation [?]. Also for our proposed method, two different scenarios are implemented: the ideal filter for which we are optimizing the spline function is first taken as a *sinc* filter, and first the spectrum of the original image. In order to evaluate the quality of the interpolated images, we have considered the Peak Signal-to-Noise Ratio (PSNR) criterion. Table I indicates the resultant PSNR values when the original image is subject to the anti-aliasing filter before down-sampling while the error is calculated based on the image without applying the filter. Table II contains similar values while the basis for the error calculation is the anti-aliased image. In both cases, the PSNR criterion favors the proposed optimized spline for the ideal lowpass (*sinc*) filter. On the average, the proposed method outperforms the other standard interpolating methods by 0.74dB in Table I and 4.19dB in Table II.

To exclude the effect of the anti-aliasing filter, the simulations are repeated without applying it and the results are presented in Table III. As expected, the optimized spline which is matched to the spectrum of the original image outperforms other competitors in all cases. It should be mentioned that the function $\rho^m[x, \rho_d^m]$ is not a universal filter in this case and depends on the choice of the image.

Although the PSNR value is a good measure of global quality of an image, it does not reflect the local properties. In order to present a qualitative view of various interpolation methods, we have plotted the enlarged images for a segment of the Lena test image in Fig. 6. To highlight the differences, one could compare the texture on the top and the sharpness on the bottom edge of the hat.

V. CONCLUSION

The interpolation problem using uniform knots is a well studied subject. In this paper, we considered the problem of

TABLE I

PSNR (dB) RESULTS OF THE RECONSTRUCTED IMAGES BY VARIOUS METHODS, THE ORIGINAL IMAGE WAS ANTI-ALIASED BEFORE SAMPLING AND THE RESULTS ARE COMPARED TO THE **ORIGINAL** IMAGE (IMAGE ENLARGEMENT FROM 256×256 TO 512×512)

Images	Bilinear	Bicubic [?]	WZP-CS [?]	SAI [?]	Optimized Spline for Image $\rho^3[x, \rho_d^3]$	Optimized Spline for the Ideal LowPass $\rho^3[sinc(t), \rho_d^3]$
Lena	30.33	30.44	30.12	30.96	32.46	32.20
Baboon	22.40	22.52	22.41	22.89	22.20	24.22
Barbara	24.39	24.42	24.34	24.65	24.33	25.14
Peppers	29.46	29.46	29.14	29.72	31.14	31.04
Girl	30.98	30.98	30.66	30.43	31.70	30.87
Fishing bout	27.68	27.48	28.12	30.92	28.61	29.71
Couple	27.35	27.50	27.27	27.39	28.04	28.97
Overall Average	27.51	27.54	27.43	28.14	28.35	28.88

TABLE II

PSNR (dB) RESULTS OF THE RECONSTRUCTED IMAGES BY VARIOUS METHODS, THE ORIGINAL IMAGE WAS ANTI-ALIASED BEFORE SAMPLING AND THE RESULTS ARE COMPARED TO THE **ANTI-ALIASED** IMAGE (IMAGE ENLARGEMENT FROM 256×256 TO 512×512)

Images	Bilinear	Bicubic [?]	WZP-CS [?]	SAI [?]	Optimized Spline for Image $\rho^3[x, \rho_d^3]$	Optimized Spline for the Ideal LowPass $\rho^3[sinc(t), \rho_d^3]$
Lena	31.56	31.72	31.62	32.45	35.28	35.21
Baboon	26.88	27.26	26.89	28.48	26.33	35.70
Barbara	30.61	30.74	30.65	31.86	30.40	35.72
Peppers	31.62	31.82	31.77	32.14	37.41	38.02
Girl	34.08	34.24	34.25	33.10	35.89	34.28
Fishing bout	29.91	30.19	29.93	30.92	32.00	34.87
Couple	29.81	30.10	29.84	29.77	31.44	34.28
Overall Average	30.64	30.87	30.71	31.25	32.68	35.44

TABLE III

PSNR (dB) RESULTS OF THE RECONSTRUCTED IMAGES BY VARIOUS METHODS, THE **ORIGINAL IMAGE WAS NOT ANTI-ALIASED** AND THE RESULTS ARE COMPARED TO THE **ORIGINAL** IMAGE 256×256 TO 512×512)

Images	Bilinear	Bicubic [?]	WZP-CS [?]	SAI [?]	Optimized Spline for Image $\rho^3[x, \rho_d^3]$	Optimized Spline for the Ideal LowPass $\rho^3[sinc(t), \rho_d^3]$
Lena	30.21	30.13	30.05	30.88	32.29	30.95
Baboon	21.67	21.34	21.70	22.09	22.50	21.63
Barbara	23.90	23.32	23.88	23.71	25.10	22.58
Peppers	28.82	28.61	26.93	28.91	30.64	29.77
Girl	30.41	29.97	30.20	29.94	30.90	29.20
Fishing bout	27.10	26.93	27.07	27.63	28.50	27.66
Couple	26.92	26.73	26.86	26.93	27.91	27.08
Overall Average	27.00	26.72	26.67	27.16	29.12	26.98

optimizing the interpolation kernel for a given class of signals (represented by a filter). Although functional optimization in the continuous domain is often very difficult, we have demonstrated the equivalency of this problem with a finite dimensional linear problem which can be easily solved using linear algebra. As a special case, we considered the class of lowpass signals which is associated with the sinc function as the optimum interpolation kernel. For the optimum compact support interpolant, we compared our function with the conventional cubic B-Spline; the simulation results indicate 1dB improvement in the SNR of the interpolated signal (on the average) using the introduced function, and 7dB improvement compared to the cardinal spline itself (compared to the sinc function) (Fig. 5).

ACKNOWLEDGMENT

The authors would like to thank Prof. M. Unser from EPFL and Dr. R. Razvan from the mathematical sciences department of Sharif university for their helpful comments.

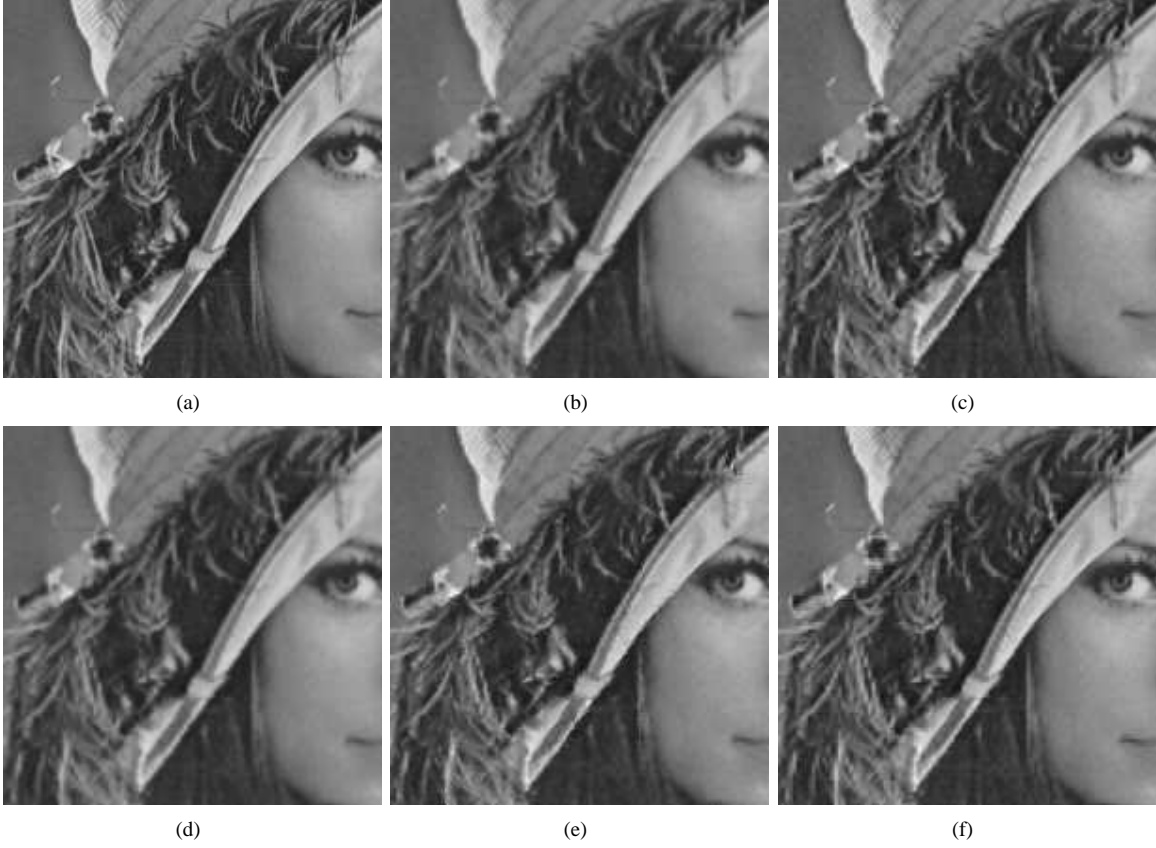


Fig. 6. Comparison of different methods for the Lena image: (a) The original image, (b) bilinear interpolation, (c) bicubic Interpolation. (d) WZP Cycle-Spinning [?], (e) SAI [?], and (f) the proposed method.